COMPARISON OF BUOYANCY AND SURFACE TENSION IN A SQUARE CAVITY

Tae-Ho Song*

(*Received October, 18, 1990*)

Laminar natural convection induced by free surface temperature gradient has been investigated numerically. Buoyancy effect and surface tension effect were made to oppose against each other. For fluid of unit Prandtl number and cavity of unit aspect ratio, the flow field was examined to determine the relative importance of surface tension force and buoyancy force. The flow patterns of each regime are : free surface-concentrated streamlines for surface tension flows, opposite direction circulation for buoyancy driven flows, and surface tension cell above with buoyancy driven cell below for mixed flows. The borderlines of each flow regime were obtained by interpolation and the flow regime map was obtained.

Key Words: Buoyancy, Flow regime, Natural Convection, Surface Tension

NOMENCLATURE

c_p : Specific heat
g : Gravitational constant
H : Cavity height
k : Thermal conductivity
L : Cavity length
p : Pressure
T : Temperature
u : Horizontal velocity
v : Vertical velocity
x : Horizontal coordinate
y : Vertical coordinate
β : Volumetric thermal expansion coefficient
μ : Dynamic viscosity
ν : Kinematic viscosity
σ : Density
θ : Dimensionless temperature
Bo : Bond number
Gr : Grashof number
Ma : Marangoni number
Pr : Prandtl number
Re : Reynolds number

1. INTRODUCTION

Recently, natural convection in a cavity in presence of free surface has been of considerable interest because of its practical applications in production of glass, metal and single crystals.

The presence of free surface in buoyancy driven natural convection system adds shear stress at the free surface due to variation of surface tension which is a strong function of temperature. The combination of buoyancy and free surface shear frequently exhibits complex flow field. These two forces may assist or compete with each other to dominate the flow field. In spite of the importance of the problem, not many publications are available yet. Most researches regading natural convection in enclosures have been about the well-known buoyancy driven free convection with different side wall temperatures(Bejan and Tien, 1978, Ozoe and Sayama, 1974, Shiralkar and Tien, 1981, Wilkes and Churchill, 1966, Cormack, Leal and Imberger, 1974a,b,c). Bergman and Keller(1988) lately reported computational results on cavity circulation with presence of free surface in liquid metal. On the other hand, Srinivasan and Basu(1986) have studied the combined natural convection with strong laser irradiation on the top of cavity numerically. These two researches show that the dominant factor of flow field may be found by comparing the magnitudes of buoyancy force and surface tension force. Their decisive dimensionless parameters are different from each other, however. The former have taken the Bond number as the decisive parameter while the latter have employed the ratio of Rayleigh number times Prandtl number to the square of Marangoni number. The detailed regime of flow pattern, in fact, has not been clearly known yet. It is the aim of this research to identify the relative importance of these two forces, thereby enabling predicting the flow pattern in advance.

Fig. 1 shows a cavity with free surface and unit aspect ratio. Liquid with unit Prandtl number is filled in and linear temperature gradient is imposed on the free surface. Both the buoyancy effect and the surface tension effect exist. Surface tension decreases as temperature increases while density of fluid decreases as temperature increases. With higher surface temperature at the right corner, the surface tension force tends to rotate the fluid in counterclockwise manner, while the buoyancy force tries to induce clockwise circulation. These two forces are, thus, competing with each other and it facilitates to discern which force is dominating the flow. This situation is taken since it is difficult to find out the relative importance of the two forces in assisting flows. This type of flow pattern is frequently found in freezing process of ice. Similar situations may be met in glass melting, metal ingot production, laser machining and single crystal production by

*Department of Mechanical Engineering, Korea Advanced Institute of Science and Technology, Taejon, 305-701, Korea

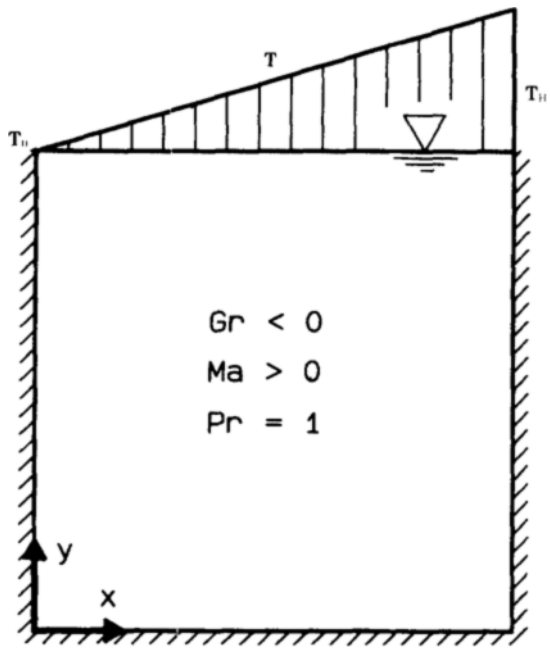

Fig. 1 Schematic of the physical system. Negative Grashof number means clockwise rotational torque by buoyancy while positive marangoni number means counterclockwise rotational torque by surface tension gradient.

Czochralski process. The other walls are taken adiabatic because this type of situation is common in real processes. It is assumed that the free surface does not have surface wave and the degree of thermal expansion is small enough to apply the Boussinesq approximation. This assumption means that the shape of the cavity remains almost square with flat free surface during convectional flow.

The governing equations and the method of numerical simulation are described in this paper. The results of numerical simulation are shown to see the relative importance of buoyancy and surface tension forces. The maximum speed of the fluid is regressed to determine the effect of the two forces. The velocity gradient at the bottom of the cell is also observed. These two factors are examined to set the borderline between the three flow regimes(buoyancy driven, surface tension driven and mixed flows) and to complete the flow regime map. A simplified criterion to compare the relative importances is also suggested.

2. BASIC EQUATIONS

The conservation equations of mass, momentum and energy in steady convection system are written as

$$\frac{\partial}{\partial x}(\rho u)+\frac{\partial}{\partial y}(\rho v)=0 \tag{1}$$

$$\frac{\partial}{\partial x}(\rho uu)+\frac{\partial}{\partial y}(\rho uv)=\mu\nabla^2 u-\frac{\partial p}{\partial x} \tag{2}$$

$$\frac{\partial}{\partial x}(\rho uv)+\frac{\partial}{\partial y}(\rho vv)=\mu\nabla^2 v-\frac{\partial p}{\partial y}-\rho g\beta(T-T_0) \tag{3}$$

$$\frac{\partial}{\partial x}(\rho uc_pT)+\frac{\partial}{\partial y}(\rho vc_pT)=k\nabla^2 T \tag{4}$$

where the Boussinesq approximation has been utilized. These equations are transformed into dimensionless form by using the following parameters.

$$\begin{aligned} u&=\frac{\nu}{L}u^* \\ p&=\rho\left(\frac{\nu}{L}\right)^2 p^* \\ \theta&=\frac{T-T_0}{T_H-T_0} \\ x&=Lx^* \\ y&=Ly^* \end{aligned} \tag{5}$$

Note that the temperature at the free surface changes linearly from T_0 at left to T_H at right. The length of cavity in x-direction is L and the height is H. However, the aspect ratio is unity so that $L=H$. Using these variables, the governing equations are changed as

$$\frac{\partial u^*}{\partial x^*}+\frac{\partial v^*}{\partial y^*}=0 \tag{6}$$

$$\frac{\partial}{\partial x^*}(u^*u^*)+\frac{\partial}{\partial y^*}(u^*v^*)=\frac{\partial^2 u^*}{\partial x^{*2}}+\frac{\partial^2 u^*}{\partial y^{*2}}-\frac{\partial p^*}{\partial x^*} \tag{7}$$

$$\frac{\partial}{\partial x^*}(u^*v^*)+\frac{\partial}{\partial y^*}(v^*v^*)=\frac{\partial^2 v^*}{\partial x^{*2}}+\frac{\partial^2 v^*}{\partial y^{*2}}-\frac{\partial p^*}{\partial y^*}-Gr\theta \tag{8}$$

$$\frac{\partial}{\partial x^*}(u^*\theta)+\frac{\partial}{\partial y^*}(u^*\theta)=\frac{1}{Pr}\left[\frac{\partial^2\theta}{\partial x^{*2}}+\frac{\partial^2\theta}{\partial y^{*2}}\right] \tag{9}$$

where the dimensionless numbers are Grashof number $Gr=\frac{g\beta(T_H-T_0)L^3}{\nu^2}$ and Prandtl number $Pr=\frac{\mu c_p}{k}$. The surface tension gradient imposes another dimensionless number. Defining $U_r=-\frac{d\sigma}{dT}(T_H-T_0)/\mu$, the Reynolds number Re and the Marangoni number Ma are give as $Re=U_mL/\nu$ and $Ma=Re/Pr$, respectively. An alternative to Marangoni number is defined as Bond number $Bo=GrPr/Ma$.

The boundary conditions as depicted in Fig. 1 are written as

$$\begin{aligned} &u^*=0 \text{ and } v^*=0 \text{ at } x^*=0,\ x=1 \text{ and } y^*=0 \\ &\frac{\partial\theta}{\partial x_n^*}=0 \text{ at } x^*=0,\ x^*=1 \text{ and } y^*=0 \\ &\frac{\partial u^*}{\partial y^*}=0,\ v^*=0 \text{ and } \theta=x^* \text{ at } y^*=H/L \end{aligned}$$

where x_n^* denotes coordinate perpendicular to the wall. The Grashof number is taken to be negative by assigning negative thermal expansion coefficient and the Marangoni number is taken to be positive by assuming that the surface tension decrease as the temperature increases. This situation is typically that of natural convection of water with free surface between 0 and 4℃. There are 3 dimensionless numbers that decide the flow field, i.e., Gr, Pr and Ma. It is anticipated that the effect of Pradtl number is not great if Pr is not far from unity. For this reason, Prandtl number is taken to be unity and the effects of the other two parameters are investigated numberically.

3. NUMRICAL SCHEME

The above equations were solved numerically using a SIMPLER algorithm(Patankar, 1980) with 40 by 40 uniform control volumes. Five hundred iterations were sufficient to converge the velocities within the error bound of less than 10^{-5}

of the maximum velocity. For surface tension driven flows, the convergence was fast while it was rather slow for buoyancy driven flows. The convergence was also slow when the Grashof number or the Marangoni number was large.

The computing time for 500 iterations was about 1200 seconds with scalar processing on a CONVEX. 1 system, a 32 bit machine. Less than 5 percent of the computing time was spent on input and output.

Two parameters are taken as the coordinates of the flow regime map, i.e., Grashof number on the horizontal axis and Marangoni number on the vertical axis. Grashof number and Marangoni number are varied along a quarter circle as given by

$$log^2 | Gr | + log^2 | Ma | = R^2 \tag{10}$$

The radius R is varied 3, 4, 5 and 6. This quarter circle is divided with equal angles into 7 segments so that the ratio $\frac{log | Ma |}{log | Gr |}$ takes values of 0.01, 0.23, 0.48, 1.25, 2.08, 4.39 and 100. Obviously, the flow pattern is expected to be surface tension dominant when this ratio is 0.01 and buoyancy dominant when it is 100. In total, thirty two cases are computed and the results are examined to determine the dominant factor.

4. EVALUATON OF NUMERICAL RESULTS

Fig. 2 shows the flow pattern of surface tension dominant flow when $Ma=1.0\times10^4$. The maximum velocity occurs at the top surface since there is no wall. The location of maximum velocity moves from about the central free surface to the left free surface as the Marangoni number increases. This is because the fluid particle is accelerated more and more as it travels along the free surface. Near the left end, however, the presence of wall suppresses further acceleration. As the Marangoni number increases, the inertia of the fluid is more dominant than the viscous shear at the free surface so that the deceleration begins later than in the case of smaller Marangoni number. This explains the elliptic shape of the recirculation cell with its longer axis stretching from right lower corner to left upper corner. At the same time, velocity variation is extremely large near the free surface and the resulting circulation cell is located close to the free surface. This makes the flow near the bottom relatively stagnant. Though it is not depicted in the streamlines (Fig. 2(a)), the velocity vector plot(Fig. 2(b)) shows two small clockwise secondary circulations near the left and right bottom corners. The magnitude of maximum velocity can be fitted as

$$u^*_{max}=0.636Ma^{0.742} \tag{11}$$

The temperature shows sharp variation along the free surface and it is fairly uniform inside the cavity (see Fig. 3). The mean temperature inside the cavity is about 0.25. The high velocity near the free surface makes the temperature in there highly nonuniform. In the meanwhile, the fairly stagnant central region exchanges thermal energy in it by diffusion to make the temperature fairly uniform. Since the free surface velocity is great near the left upper corner, the thermal boundary layer at the free surface does not grow in the same manner as in the case of uniform surface velocity. Generally speaking, the thickness of the thermal boundary layer is thin

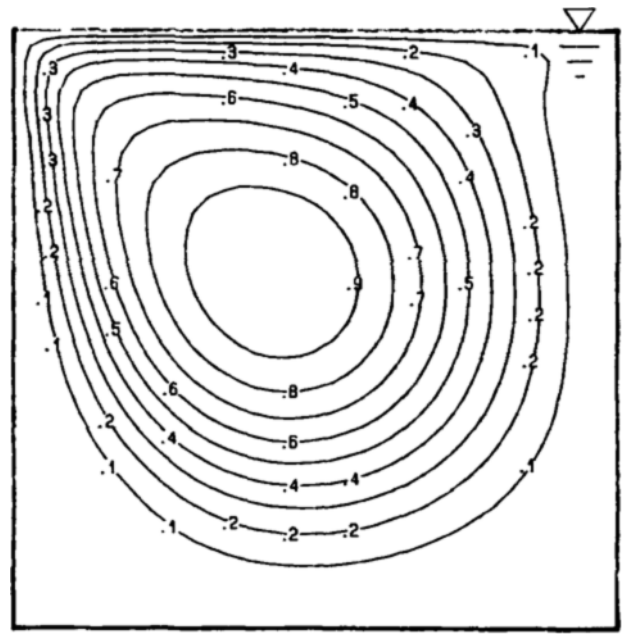

(a) Streamlines. numbers on the contour denote relative magnitudes of the stream functions between the minimum (zero) and the maximum (unity).

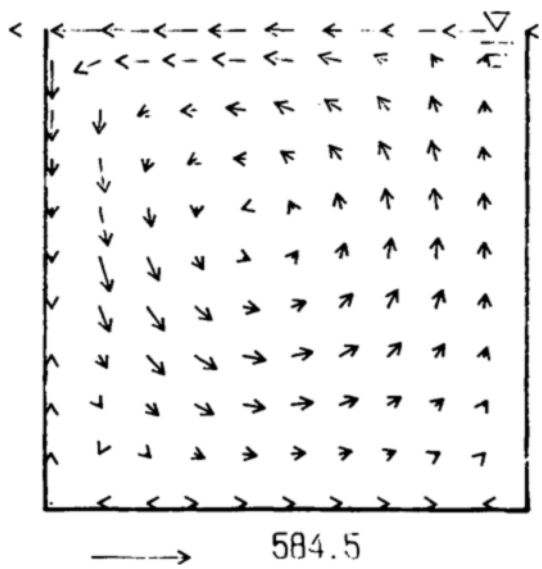

(b) Velocity vectors. the scale shows dimensionless velocity magnitude.

Fig. 2 Pattern of surface tension flow for $Ma=1.0\times10^4$ and $Gr=0$

where the free surface velocity is high. Surface temperature diffuses more effectively into the medium at the interface where the thermal boundary layer is thin. Consequently, the inside temperature of the cavity is more affected by the temperature of the surface where the velocity is greater. The fact that the mean temperature of the cavity is close to the left surface can be understood by this argument.

When the flow is buoyancy dominant, the maximum speed occurs slightly below the free surface where the dimensionless coordinate x^* is between 0.5 and 1.0 (see Fig. 4). The

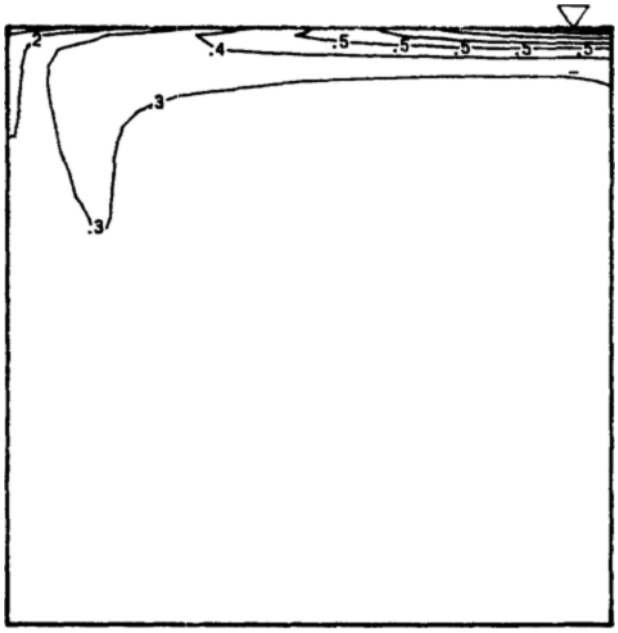

Fig. 3 Dimensionless temperature distribution for $Ma=1.0\times10^4$ and $Gr=0$. The numbers on the contour are the dimensionless temperatures.

flow field covers almost entire region while the streamlines of surface tension driven flow are compressed near the free surface. Note that the ellipses of stream lines are compressed to span more from right top surface to left lower corner. This phenomena also can be explained by the same argument as in the surface tension dominant flows. The degree of elliptic stretching of the recirculation cell and the concentration of the streamline near the free surface is, however, as great as in the case of surface tension dominant flows. This can be explained by two factors ; frst, the driving force of the natural convection in the case of buoyancy driven flow is the temperature itself, while in the surface tension driven flows, the driving force exerts only at the free surface by the temperature gradient. Consequently, the flow field is subject to driving force even deep in the cavity so that the velocity field is more uniform than in the case of surface tension driven flows. Thus, the existence of secondary recirculation cells near the lower left and right corners is not very discemible until the Grashof number is sufficiently large. Second, the maximum speed in the flow is smaller than the previous case. The smaller acceleration near the free surface reduces the elliptic stretching of the primary cell. More specifically, the maximum speed in the flow field is fitted into

$$u^*_{max}=0,0982\mid Gr\mid^{0.537} \tag{12}$$

As can be seen form the isothermal lines in Fig. 5, the temperature of the fluid is generally higher than 0.5. The fluid is heated as it travels from left to right just below the free surface and then returns down to the middle of cavity. Here again, the thermal boundary layer is thin where the surface velocity is the maximum and it explains why the mean temperature is slightly above 0.5. However, since the velocity is lower than in the case of surface tension driven flow, the variation of temperature is stretching deep into the cavity. The temperature distribution is somewhat similar to pure

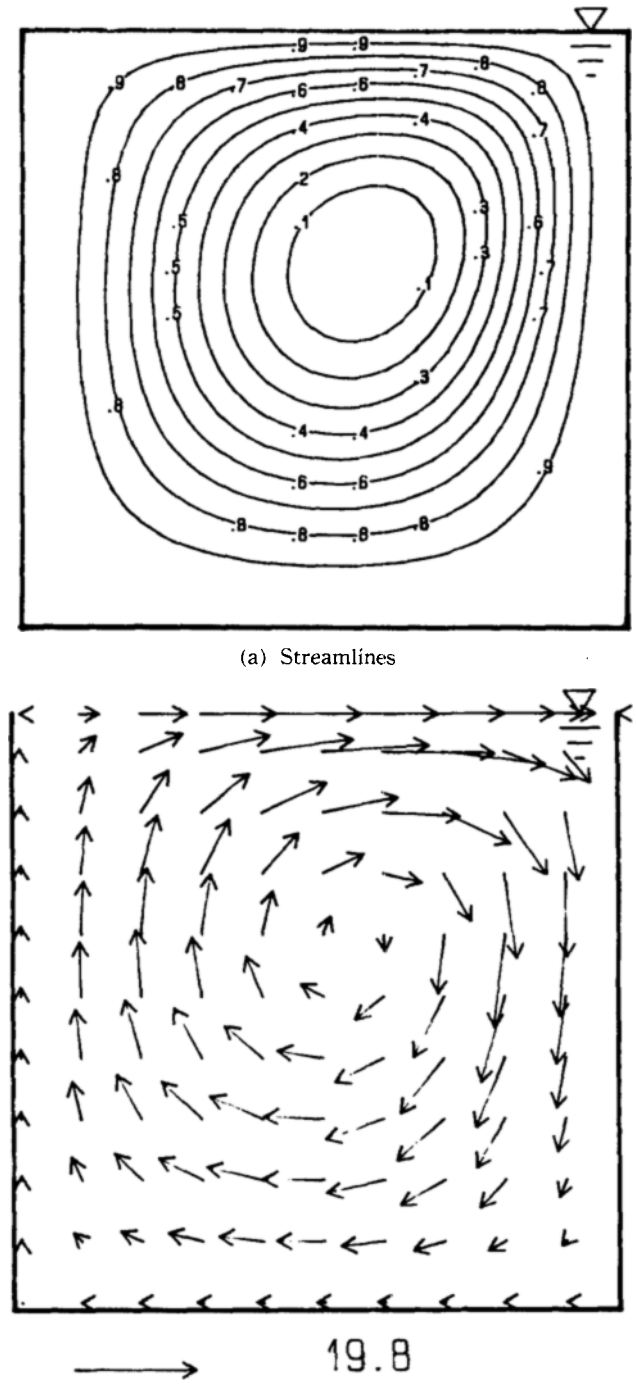

(a) Streamlines

(b) Velocity vectors

Fig. 4 Pattern of buoyancy driven flow for $Gr=-1.0\times10^{-4}$ and $Ma=0$

conduction with some distortion by convectional flow.

When the magnitudes of Gr and Ma are comparable, mixed flow pattern is observed as shown in Fig. 6. Surface tension driven flow exists near the free surface and buoyancy driven flow is located below it. The former occupies about upper one thirds of the cavity and the latter occupies the rest. Though the area of the occupied region by the surface tension cell is smaller, it exhibits greater flow velocity. The magnitude of typical velocity is, however, much smaller than

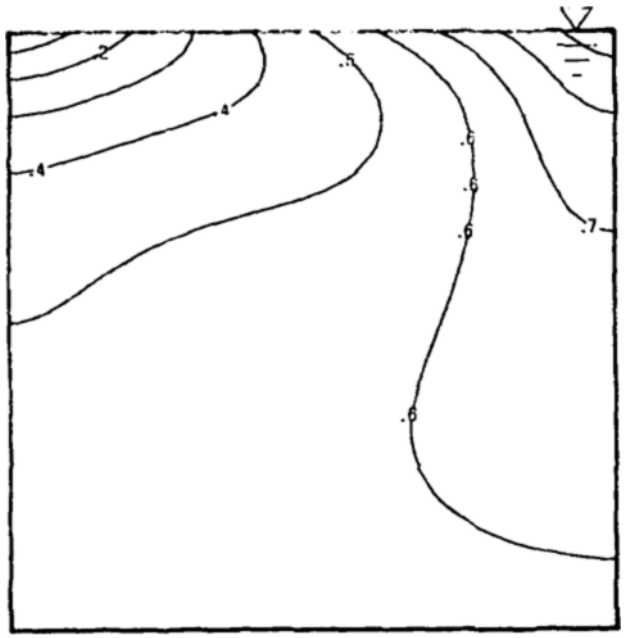

Fig. 5 Dimensionless isotherms for $Gr=-1.0\times10^4$ and $Ma=0$.

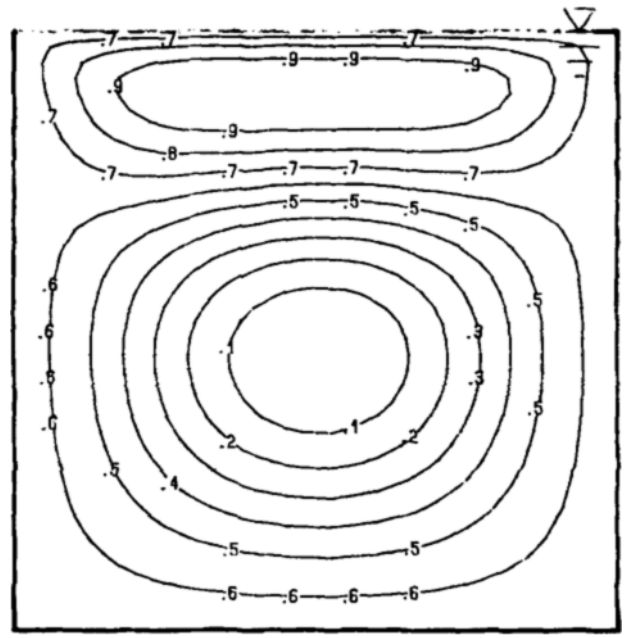

(a) Streamlines

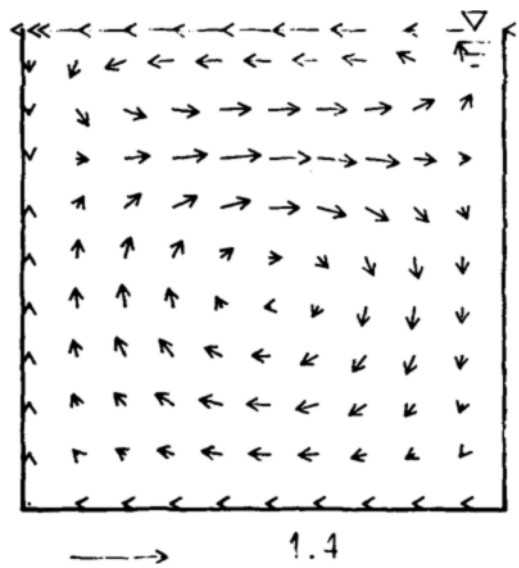

(b) Velocity vectors

Fig. 6 Mixed flow pattern for $Gr=-507$ and $Ma=20$

those of the former two cases because of the relatively small Ma and Gr, and in addition, because of the mutually competing (and thus, compensating) rotational torques. The mean temperature is dominated by the flow field at the interface, thus it is closer to the surface tension driven flow than to the buoyancy driven flow (see Fig. 7). The isothermal line of $\theta=0.2$ is bulged downward like in Fig. 3 and those of $\theta\geq0.3$ are shifted to the right due to the counterclockwise rotation of the upper cell. The lower cell has so small velocity that it hardly changes conduction-like isothermal lines. However, the process of being heated as the fluid travels to the fleft along the interface of the upper and lower cells and being cooled as it returns back to the left lower corner is obviously depicted.

The borderline of buoyancy driven flow and mixed flow may be set where the maximum velocity at the free surface is equal to zero, since it indicates whether the surface tension driven recirculation cell appears at the free surface or not. Similarly, the borderline of mixed flow and surface tension driven flow is set where the velocity gradient at the center of bottom is zero, i.e., $\frac{\partial u^*}{\partial y^*}=0$ at $X^*=0.5$ and $y^*=0$. If the gradient is negative, the clockwise buoyancy driven cell appears at the bottom. The interpolated results are summarized in Fig. 8. It shows that the ratio Ma/Gr may be used as a rough measure of deciding which flow pattern is to appear. However, the borderline is bent more and more horizontally as the magnitude of Marangoni number or Grashof number increases.

Complete verification of the existence of mixed flow in region Ⅱ is not executed in this study, rather, the borderlines are obtained by interpolation from the tested cases. The region Ⅱ, therefore, may be understood as the uncertainty interval between regions I and Ⅲ. One may even neglect region Ⅱ and set the rough borderline between the two extreme flows simply by comparing the maximum speeds. In this practice, one equates the maximum velocities by surface tension flow and buoyancy diriven flow. The result is

$$|Gr|=32.4\,|Ma|^{1.382} \tag{13}$$

When the left hand side is much alrger than the right, then it can be expected to be buoyancy driven flow, and vice versa. This result shows that neither of the two references(Bergaman and Keller, 1988, Srinivasan and Basu, 1986) correctly compares the effects of the two forces. A new criterion should be used to check the flow regime. However, it is apparent that the surface tension is more dominant than the buoyancy if the magnitudes of Ma and Gr are about the same.

It seems appropriate to point out the possibility of turbulence. Though the numerical computation was stable in the tested region, it became more or less unstable when larger number of Gr or Ma was tried. It is not clear whether it indicates the real physical instability that causes the onset of turbulence. However, it is believed that the stable computa-

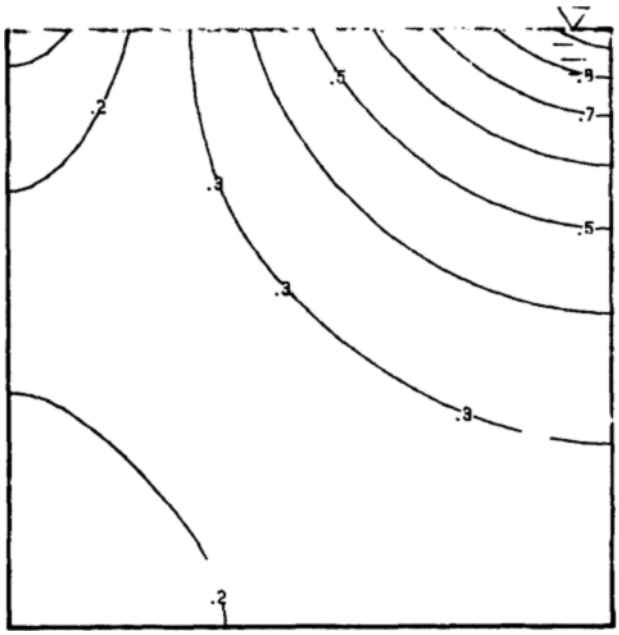

Fig. 7 Temperature distribution in the mixed flow of Fig. 6.

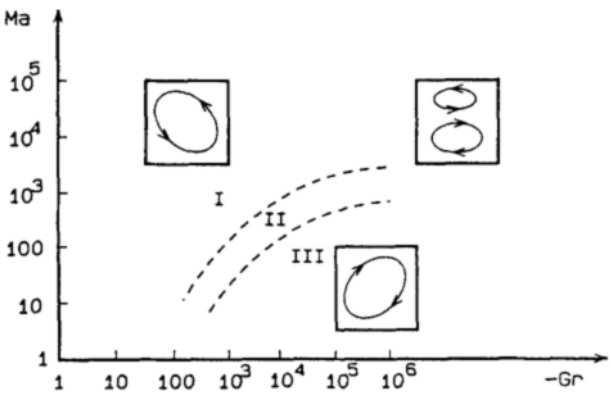

Fig. 8 Flow regimes. I; Surface tension flow regime, Ⅱ ; Mixed flow regime, Ⅲ ; Buoyancy driven flow regime.

tion in the tested region indicates that the tested region is in laminar region. This argument is supported by that the SIMPLER algorithm is making use of unsteady-like scheme in the iteration procedure (Patankar, 1980). If the flow had been turbulent, the direct numerical simulation of the Navier-Stokes equation must have shown numerical fluctuation. Since such fluctuation did not occur in the numerical computation, one might say that the tested region is in laminar region.

5. CONCLUSIONS

The regimes of surface tension driven flow, buoyancy driven flow and mixed flow are identified for the case of unit Prandtl number and unit aspect ratio. The surface tension driven flow occurs when the Marangoni number is sufficiently greater than the Grashof number. The surface tension driven flow concentrates the streamlines near the free surface and the mean temperature is close to the free surface temperature where the velocity is maximum. With Grashof number much greater than Marangoni number, the flow field is affected by buoyancy force. Maximum velocity occurs slightly below the free surface with deep penetration of flow field into the cavity. The mean temperature of the liquid is also very close to the surface temperature where the velocity is maximum. When the magnitudes of the two driving forces are comparable, mixed convection may occur. Surface tension driven cell is located near the free surface and the buoyancy driven cell is located below it. The magnitude of velocity is greater in the upper cell, however, the size of cell is greater for the lower cell. The temperature distribution of mixed convection is similar to the surface tension driven flow.

By checking the conditions of existence of the buoyancy cell and the surface tension cell, the borderlines of buoyancy driven flow/ mixed flow and surface tension flow/mixed flow have been plotted for two parameters of Ma and Gr. A simpler criterion to check the possibility of two extreme cases has also been suggested.

In this analysis, only the case of unit Prandtl number and unit aspect ratio has been investigated. If the problem under consideration has fairly different parameters, the results shown in here cannot be applied directly. Further study for different Pradtl numbers and different aspect ratios is recommended. In addition, the onset of turbulence in this type of flow needs be studied. All the computational results should be vertified through experiments.

REFERENCES

Bejan, A. and Tien, A.L., 1978, "Laminar Natural Convection Heat Transfer in a Horizontal Cavity with Different End Temperatures," J. of Heat Transfer, Vol. 100, pp. 641~646.

Bergman, T.L. and Keller, J.R., 1988, "Combined Buoyancy, Surface Tesion Flow in Liquid Metals," Numerical Heat Transfer, Vol. 13, pp. 49~63.

Cormack, D.E., Leal, L.G. and Imberger, J., 1974a, "Natural Convection in a Shallow Cavity with Differentially Heated End Walls. Part 1. Asymptotic Theory," J.Fluid Mechanics, Vol. 65, Part 3, pp. 209~229.

Cormack, D.E., Leal, L.G. and Imberger, J., 1974b, "Natural Convection in a Shallow Cavity with Differentially Heated End Walls. Part 2. Numerical Solutions," I.Fluid Mechanics, Vol. 65, Part 3, pp. 231~246.

Cormack, D.E., Leal, L.G. and Imberger, J., 1974c, "Natural Convection in a Shallow Cavity with Differentially Heated End Walls. Part 3. Experimental Results," J.Fluid Mechanics, Vol. 65, Part 3, pp. 247~260.

Ozoe, H. and Sayama, H., 1974, "Natural Convection in Inclined Square Channel," Int. J. Heat Mass Transfer, Vol. 17, pp. 401~406.

Patankar, S.V., 1980, "Numerical Heat Transfer and Fluid Flow," McGraw-Hill, New York.

Shiralkar, G.S. and Tien, C.L., 1981, "A Numerical Study of Laminar Natural Convection in Shallow Cavities," J. Heat Transfer, Vol. 103, pp. 226~231.

Srinivasan, J. and Basu Biswajit., 1986, "A Numerical Study of Thermocapillary Flow in a Rectangular Cavity During Laser Melting," Int. J. Heat Mass Transfer, Vol. 29, No. 4, pp. 563~572.

Wilkes, J.O. and Churchill, S.W., 1966, "The Finite-Difference Computation of Natural Convection in a Rectangular Enclosure," A.I.Ch.E., Journal, Vol.12, No.1, pp. 161~166.